Biophysical Chemistry 180–181 (2013) 22–28

Contents lists available at ScienceDirect

Biophysical Chemistry

journal homepage: http://www.elsevier.com/locate/biophyschem

Translocation dynamics of tRNA–mRNA in the ribosome

Ping Xie

Key Laboratory of Soft Matter Physics and Beijing National Laboratory for Condensed Matter Physics, Institute of Physics, Chinese Academy of Sciences, Beijing 100190, China

HIGHLIGHTS

- A model for EF-G-catalyzed tRNA–mRNA translocation is proposed.
- EF-G.GTP can also bind to classical non-rotated PRE state besides hybrid state.
- Greater potency of EF-G with GTP than GDPNP in catalyzing translocation derives from effect on hybrid-to-POST transition.

GRAPHICAL ABSTRACT

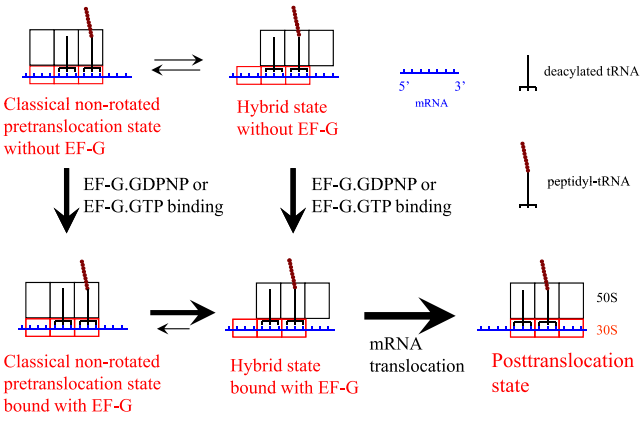

ARTICLE INFO

Article history:
Received 1 May 2013
Received in revised form 30 May 2013
Accepted 1 June 2013
Available online 13 June 2013

Keywords:
Ribosome
Translocation
Hybrid state
Translation
tRNA–mRNA

ABSTRACT

Translocation of tRNA–mRNA complex in the ribosome is an essential step in the elongation cycle of protein synthesis. However, some important issues concerning the molecular mechanism of the tRNA–mRNA translocation catalyzed by EF-G.GTP or by EF-G.GDPNP remain controversial. For example, can EF-G.GTP selectively bind to the hybrid pretranslocation state or bind to both the non-rotated pretranslocation and the hybrid pretranslocation states? Does the greater potency of EF-G in the presence of GTP rather than GDPNP in facilitating translocation derive from the effects on transition from the classical non-rotated to hybrid state (the first step of the translocation) or on transition from the hybrid to posttranslocation state (the second step)? Here, based on our proposed model, we study theoretically the dynamics of the tRNA–mRNA translocation through the ribosome catalyzed by EF-G.GTP and by EF-G.GDPNP. By comparing our theoretical results with the available experimental data, we show that EF-G.GTP can also bind to the classical non-rotated pretranslocation state and the greater potency of GTP hydrolysis in facilitating translocation of tRNA–mRNA complex derives from its effects on the second step of the translocation process.

1. Introduction

Translocation is an essential step of the elongation cycle of the protein synthesis in which tRNA and mRNA are moved through the ribosome. It is generally believed that the translocation takes place via two steps [1,2]. First, peptidyl-tRNA and deacylated tRNA are transited between classical

E-mail address: pxie@aphy.iphy.ac.cn.

0301-4622/$ – see front matter © 2013 Elsevier B.V. All rights reserved.
http://dx.doi.org/10.1016/j.bpc.2013.06.001

non-rotated (A/A and P/P sites, respectively) and hybrid (A/P and P/E sites, respectively) states [3–12]. Then, catalyzed by elongation factor EF-G in the presence of GTP, the two tRNA molecules that are coupled with mRNA via codon–anticodon interaction are transited from the hybrid to posttranslocation (P/P and E/E sites) states. It has been shown that GTP hydrolysis accelerates the second step by promoting the "unlocking" rearrangement of the ribosome [13]. Moreover, EF-G.GDPNP (GDPNP is a nonhydrolyzable analog of GTP) can also activate the translocation of tRNA–mRNA complex, but with a lower translocation rate than that catalyzed by EF-G.GTP [12,14–18]. Despite the intensive and extensive studies, the detailed molecular mechanism of the tRNA–mRNA translocation catalyzed by EF-G.GTP or by EF-G.GDPNP remains elusive and some important issues concerning the mechanism are controversial. For example, can EF-G.GTP selectively bind to the hybrid state or bind to both the non-rotated pretranslocation and the hybrid states [8,11]? Does the greater potency of EF-G in the presence of GTP rather than GDPNP in facilitating translocation derive from the effects on the first step or on the second step of the translocation process [11,13,16,18]?

In this work, based on our proposed model we study theoretically the dynamics of tRNA–mRNA translocation catalyzed by EF-G.GTP and by EF-GDPNP. We show that with the consideration that EF-G.GTP can bind to both the non-rotated pretranslocation and the hybrid states of the ribosomal complex, the theoretical results are in good agreement with the available experimental data [16]. However, with the consideration that EF-G.GTP can selectively bind to the hybrid state, the theoretical results are sharply different from the experimental data [16]. Moreover, the available experimental data on translocation catalyzed by EF-G.GDPNP [16] can also be quantitatively explained by the consideration that EF-G.GDPNP mainly has a different effect from EF-G.GTP on the transition from the hybrid to posttranslocation states. Thus, the studies in this work give a strong support to the argument that EF-G.GTP can bind to both the non-rotated pretranslocation and the hybrid state of the ribosomal complex and indicate that the greater potency of GTP hydrolysis in facilitating translocation of tRNA–mRNA complex derives from its effects on the transition from the hybrid to posttranslocation states – the second step of the tRNA–mRNA translocation process – rather than on the hybrid-state formation – the first step of the translocation process.

2. Methods

2.1. Model

For simplicity, in the model we consider only three states of the ribosomal complex and two conformations of the ribosome during translocation from the pretranslocation to posttranslocation states. The three states include non-rotated pretranslocation, hybrid and posttranslocation states and the two conformations are called the non-rotated and rotated. In the non-rotated pretranslocation and posttranslocation states the ribosome is in the non-rotated conformation, while in the hybrid state the ribosome is in the rotated conformation.

Before binding of EF-G.GTP or EF-G.GDPNP to the ribosomal complex, the mRNA channel in 30S subunit is tight and thus the 30S subunit has a high affinity for the tRNA–mRNA complex. As a result, the tRNA–mRNA complex is kept fixed to the 30S subunit while the ribosomal complex fluctuates spontaneously forth and back between the classical non-rotated pretranslocation state (State C0, Fig. 1) and the hybrid state (State H0, Fig. 1), with the two states in equilibrium with each other [3–12]. The binding of EF-G.GTP or EF-G.GDPNP shifts the equilibrium toward the hybrid state [8–12,19], where we denote the classical non-rotated pretranslocation state and hybrid state bound with EF-G by State C and State H, respectively, in order to distinguish State C0 and State H0 without EF-G. Here it is argued that the binding of EF-G.GTP or EF-G.GDPNP reduces the interaction of the 30S subunit with the tRNA–mRNA complex. The argument is inferred from the following available experimental results. EF-G activates the translocation of tRNA–mRNA in the presence of GTP and GDPNP, whereas the translocation rarely occurs in the absence of EF-G [18,19]. Moreover, the binding of EF-G.GDPNP promotes mRNA back-slippage [19], implying the reduction of the interaction of the 30S subunit with the tRNA–mRNA complex.

Based on the argument, we have the following deduction for the case of EF-G.GDPNP binding. During reverse ribosomal rotation from the rotated (in hybrid state) to non-rotated conformations, either the two tRNAs can move relative to the 50S subunit while the tRNA–mRNA complex is kept fixed to the 30S subunit by the intermediate affinity between them (transition from State H to State C, Fig. 1) or the two tRNAs together with mRNA via codon–anticodon interaction move relative to the 30S subunit while the two tRNAs are fixed to the 50S subunit due to the specific affinity of the 50S E site for deacylated tRNA and that of the 50S P site for the peptidyl-tRNA [4,20,21] (transition from State H to State POST, Fig. 1). Thus, the movement time of the tRNA–mRNA complex from the hybrid to posttranslocation state for the case of EF-G.GDPNP binding is determined by the time required to overcome the intermediate affinity of the 30S subunit for the tRNA–mRNA complex.

For the case of EF-G.GTP binding, it is further argued that EF-G.GTP hydrolysis induces unlocking of the ribosome, which detaches the mRNA–tRNA complex from the decoding center in the 30S subunit.

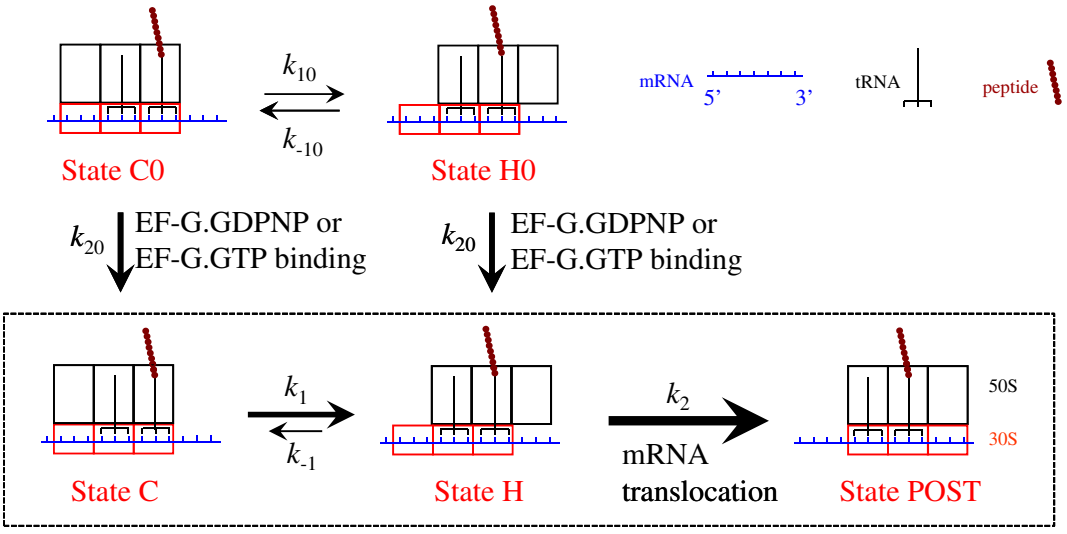

Fig. 1. Model for tRNA–mRNA translocation through the ribosome.

The argument is based on the following experimental evidence. Biochemical data showed that EF-G.GTP hydrolysis drives a conformational rearrangement of the ribosome (referred to as unlocking of the ribosome) that precedes and limits the rate of tRNA–mRNA translocation [13]. Structural studies indicated that after EF-G.GTP hydrolysis smaller conformational changes in EF-G cause a shift of domain IV toward the decoding center, which could detach the mRNA–tRNA complex from the decoding center [22,23]. After the detachment of the tRNA–mRNA complex from the decoding center in the 30S subunit, since the 30S site has nearly no affinity for the tRNA–mRNA complex, the complex can rapidly move relative to the 30S subunit. As it has been calculated, the movement time for this case is only several milli-seconds (Xie, unpublished results), which is much shorter than the time of GTP hydrolysis and then the unlocking of the ribosome [13,24]. Moreover, since GTP hydrolysis rate is much larger than the unlocking rate [13,24], the mRNA translocation time for this case is approximately determined by the time of the ribosomal unlocking.

Thus, based on our model the smaller rate of mRNA–tRNA translocation for the case of EF-G.GDPNP binding than for the case of EF-G.GTP binding is due to the fact that the time required to overcome the intermediate affinity of the 30S subunit for the tRNA–mRNA complex in the former case is longer than the ribosomal unlocking time in the latter case.

2.2. Equations at saturating EF-G.GTP

At saturating EF-G.GTP, the model shown in Fig. 1 is reduced to that shown inside the box of Fig. 1. If we denote by P_1, P_2 and P_3 the probabilities of State C, State H and State POST, respectively, from Fig. 1 (inside the box) the temporal evolutions of the three probabilities $P_1(t)$, $P_2(t)$ and $P_3(t)$ are described by the following equations

$$\frac{dP_1(t)}{dt} = -k_1P_1(t) + k_{-1}P_2(t), \tag{1}$$

$$\frac{dP_2(t)}{dt} = k_1P_1(t) - (k_{-1} + k_2)P_2(t), \tag{2}$$

$$\frac{dP_3(t)}{dt} = k_2P_2(t), \tag{3}$$

where k_1 is the rate of transition from State C to State H, k_{-1} the rate of inverse transition from State H to State C and k_2 the rate of transition from State H to State POST, as shown in Fig. 1. The initial conditions at $t = 0$ are as follows: $P_1(0) = 1$, $P_2(0) = P_3(0) = 0$. Solving Eqs. (1)–(3) we finally obtain

$$P_1(t) = -\frac{(k_{-1} + k_2 + \lambda_1)}{\lambda_2 - \lambda_1}e^{\lambda_1 t} + \frac{(k_{-1} + k_2 + \lambda_2)}{\lambda_2 - \lambda_1}e^{\lambda_2 t}, \tag{4}$$

$$P_2(t) = -\frac{k_1}{\lambda_2 - \lambda_1}e^{\lambda_1 t} + \frac{k_1}{\lambda_2 - \lambda_1}e^{\lambda_2 t}, \tag{5}$$

$$P_3(t) = -\frac{k_1k_2}{\lambda_1(\lambda_1 - \lambda_2)}\left(1 - e^{\lambda_1 t}\right) + \frac{k_1k_2}{\lambda_2(\lambda_1 - \lambda_2)}\left(1 - e^{\lambda_2 t}\right), \tag{6}$$

where

$$\lambda_1 = -\frac{(k_1 + k_{-1} + k_2)}{2} + \frac{\sqrt{(k_1 + k_{-1} + k_2)^2 - 4k_1k_2}}{2}, \tag{7}$$

$$\lambda_2 = -\frac{(k_1 + k_{-1} + k2)}{2} - \frac{\sqrt{(k_1 + k_{-1} + k_2)^2 - 4k_1k_2}}{2}. \tag{8}$$

Changes in fluorescence of prf-labeled tRNAs in experiments of Pan et al. [16] can be calculated by

$$CF = B_1P_1(t) + B_2P_2(t) + B_3P_3(t), \tag{9}$$

where B_1, B_2 and B_3 are constants which represent fluorescence intensities of prf-labeled tRNAs at State C, State H and State POST, respectively. Substituting Eqs. (4)–(6) into Eq. (9) we have

$$CF = A_1e^{\lambda_1 t} + A_2e^{\lambda_2 t} + A_3, \tag{10}$$

$$A_1 = -\frac{k_1}{\lambda_2 - \lambda_1}\left[\frac{B_1(k_{-1} + k_2 + \lambda_1)}{k_1} + B_2 + \frac{B_3k_2}{\lambda_1}\right], \tag{11}$$

$$A_2 = \frac{k_1}{\lambda_2 - \lambda_1}\left[\frac{B_1(k_{-1} + k_2 + \lambda_2)}{k_1} + B_2 + \frac{B_3k_2}{\lambda_2}\right], \tag{12}$$

$$A_3 = B_3\frac{k_1k_2}{\lambda_1\lambda_2} = B_3. \tag{13}$$

From Eqs. (7) and (8) it is seen that λ_1 and λ_2 have negative values and $|\lambda_2| > |\lambda_1|$. From Eqs. (11)–(13) it is easily obtained that $CF = B_1$ at $t = 0$ and $CF = B_3$ at $t = \infty$. The maximum value of CF occurs at

$$t_{\max} = \frac{\ln\left(\frac{(k_{-1}+k_2+\lambda_1)\lambda_1 + k_1\lambda_1B_2/B_1 + k_1k_2B_3/B_1}{(k_{-1}+k_2+\lambda_2)\lambda_2 + k_1\lambda_2B_2/B_1 + k_1k_2B_3/B_1}\right)}{\lambda_2 - \lambda_1}, \tag{14}$$

and the maximum value of CF is calculated by

$$CF_{\max} = A_1e^{\lambda_1 t_{\max}} + A_2e^{\lambda_2 t_{\max}} + A_3. \tag{15}$$

2.3. Equations at non-saturating EF-G.GTP

We denote by P_{10} and P_{20} the probabilities of State C0 and State H0 before the binding of EF-G.GTP, respectively. As in the above section, we still denote by P_1 and P_2 the probabilities of State C and State H after the binding of EF-G.GTP, respectively, and P_3 the probability of State POST. From Fig. 1, the temporal evolutions of the probabilities $P_{10}(t)$, $P_{20}(t)$, $P_1(t)$, $P_2(t)$ and $P_3(t)$ are described by the following equations

$$\frac{dP_{10}(t)}{dt} = -(k_{10} + k_{20})P_{10}(t) + k_{-10}P_{20}(t), \tag{16}$$

$$\frac{dP_{20}(t)}{dt} = k_{10}P_{10}(t) - (k_{-10} + k_{20})P_{20}(t), \tag{17}$$

$$\frac{dP_1(t)}{dt} = k_{20}P_{10}(t) - k_1P_1(t) + k_{-1}P_2(t), \tag{18}$$

$$\frac{dP_2(t)}{dt} = k_{20}P_{20}(t) + k_1P_1(t) - (k_{-1} + k_2)P_2(t), \tag{19}$$

$$\frac{dP_3(t)}{dt} = k_2P_2(t), \tag{20}$$

where k_{10} is the rate of transition from State C0 to State H0 and k_{-10} the rate of inverse transition from State H0 to State C0, as shown in Fig. 1, $k_{20} = k_b$[EF-G], with k_b representing the binding rate of EF-G.GTP and [EF-G] representing the concentration of EF-G.GTP. The initial conditions at $t = 0$ as follows: $P_{10}(0) = 1$, $P_{20}(0) = P_1(0) = P_2(0) = P_3(0) = 0$.

Now, the change in fluorescence of prf-labeled tRNAs in experiments of Pan et al. [16] can be calculated by

$$CF = B_1[P_{10}(t) + P_1(t)] + B_2[P_{20}(t) + P_2(t)] + B_3P_3(t), \tag{21}$$

where B_1, B_2 and B_3 are constants which represent fluorescence intensities of prf-labeled tRNAs at classical non-rotated pretranslocation state, hybrid state and posttranslocation state, respectively.

3. Results

3.1. In the presence of saturating EF-G.GTP

From Eqs. (10)–(13), it is clearly seen that the fluorescence intensity of prf-labeled tRNAs versus time has a double-exponential form, which is consistent with the experimental data [16].

The analytical results of $CF = B_1$ at $t = 0$ and $CF = B_3$ at $t = \infty$ imply that the fluorescence intensity of prf-labeled tRNAs observed at $t = 0$ corresponds to that at the non-rotated pretranslocation state, and the intensity at $t = \infty$ corresponds to that at the posttranslocation state, as suggested by Pan et al. [16]. However, from Eqs. (14) and (15) it is seen that the maximum fluorescence intensity is the combination of the intensities at the non-rotated pretranslocation, intermediate hybrid and posttranslocation states rather than only the intensity at the intermediate hybrid state, which is different from that suggested by Pan et al. [16].

To see the maximum fluorescence intensity CF_{max} as functions of B_2/B_1 and B_3/B_1, we first choose values of state-transition rates k_1, k_{-1} and k_2 (see Table 1). Available experimental data showed that the binding of EF-G.GTP or EF-G.GDPNP shifts the equilibrium toward the hybrid state of the labile ribosome [8–12,19], indicating that k_1 has a much larger value than k_{-1}. Thus, we take $k_1 = 8\ s^{-1}$ and $k_{-1} = 0.1\ s^{-1}$. Note that the value of k_1 is consistent with the available experimental data [7,8,25], and provided that k_{-1} is small, the change of the value of k_{-1} has a very small effect on the results (see Fig. S1 in Supplementary material). As the rate of GTP hydrolysis is much larger than the rate of ribosomal unlocking [13,24], the value of k_2 is approximately only determined by the rate of ribosomal unlocking. From the available experimental data for the rate of ribosomal unlocking [13,24], we take $k_2 = 20\ s^{-1}$ here.

From the experimental data (see Fig. 1B, C and D in Pan et al. [16]), we have $B_3/B_1 = 1.09$, 1.13 and 0.9 for the three labeled PRE complexes 16/17A, 16/20A and 20P, respectively. Using Eqs. (14) and (15) we calculate time t_{max} at which the maximum fluorescence intensity can occur and the maximum fluorescence intensity CF_{max} versus B_2/B_1 for the three labeled PRE complexes. The results are shown in Fig. 2. It is seen that for PRE complex 16/17A ($B_3/B_1 = 1.09$), only when $B_2/B_1 \geq 1.23$ can the maximum fluorescence intensity exist that is larger than B_3 at $t = \infty$. In other words, it is required that $B_2/B_1 < 1.23$ for the fluorescence intensity at any time to be smaller than B_3 at $t = \infty$. For PRE complex 16/20A ($B_3/B_1 = 1.13$), it is required that $B_2/B_1 \geq 1.33$ for the maximum fluorescence intensity to exist that is larger than B_3 at $t = \infty$. For PRE complex 20P ($B_3/B_1 = 0.9$), it is required that $B_2/B_1 > 1$ for the maximum fluorescence intensity to exist that is larger than B_1 at $t = 0$.

By comparison, the fraction of fMetPhe-puromycin formation (i.e., peptidyl-tRNA reactivity toward puromycin) versus time, as studied in Pan et al. [16], can be characterized by the probability of posttranslocation state, $P_3(t)$, versus time. This is because fMetPhe-tRNA^{Phe} (i.e., the peptidyl-tRNA) reacts with puromycin to form fMetPhe-puromycin at a rate that is 10^3–10^4-fold slower when it is bound in a pretranslocation ribosomal complex than when it is bound in a posttranslocation complex and thus, the contribution of the pretranslocation states (State C and State H) to the fMetPhe-puromycin formation can be negligible. From Eq. (6) it is easily shown that the probability of the posttranslocation state is 0 at $t = 0$ and 1 at $t = \infty$, and the maximum probability that is larger than 1 at $t = \infty$ does not exist, implying that the fraction of fMetPhe-puromycin formation at any time is smaller than that at $t = \infty$, which is in agreement with the experimental data (see Fig. 1A in Pan et al. [16]).

Table 1
Values of state-transition rates used in the calculations.

Transition rates	Binding of EF-G.GTP	Binding of EF-G.GDPNP
k_{10} (s^{-1})	0.1	0.1
k_{-10} (s^{-1})	0.1	0.1
k_b ($\mu M^{-1}\ s^{-1}$)	8	1
k_1 (s^{-1})	8	8
k_{-1} (s^{-1})	0.1	0.1
k_2 (s^{-1})	20	2

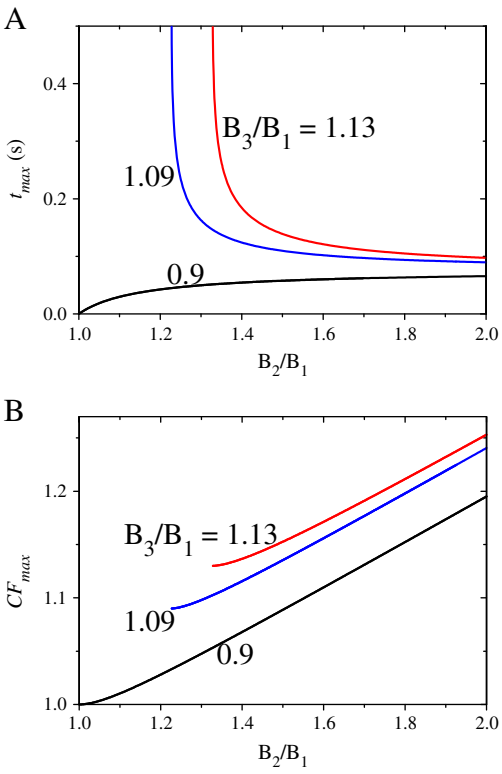

Fig. 2. Conditions under which the maximum fluorescence intensity can occur at saturating EF-G.GTP. (A) Time t_{max} at which the maximum fluorescence intensity can occur and (B) the maximum fluorescence intensity CF_{max} versus B_2/B_1 for three labeled PRE complexes 16/17A (with $B_3/B_1 = 1.09$), 16/20A (with $B_3/B_1 = 1.13$) and 20P (with $B_3/B_1 = 0.9$).

3.2. In the presence of non-saturating EF-G.GTP

At non-saturating EF-G.GTP, the temporal evolutions of state probabilities are described by Eqs. (16)–(20). The equations are complicated that it is difficult to derive the analytical forms of state probabilities versus time. Thus, we solve Eqs. (16)–(20) numerically by using the Runge–Kutta method to obtain the temporal evolutions of the state probabilities. From the equations it is noted that besides parameters k_1, k_{-1} and k_2, as discussed above, there are also three parameters: rates k_{10} and k_{-10} of transitions between the non-rotated pretranslocation and hybrid states in the absence of EF-G-GTP, and the EF-G.GTP-binding rate $k_{20} = k_b$ [EF-G], where [EF-G] represents the concentration of EF-G.GTP. We take $k_{10} = k_{-10} = 0.1\ s^{-1}$ (Table 1), which is consistent with the experimental data of Cornish et al. [9]. We take $k_b = 8\ \mu M^{-1}\ s^{-1}$ (Table 1), which is close to that obtained from dye-labeled tRNA assays [26,27]. As it will be seen below, with these values of k_{10}, k_{-10} and k_b, the calculated results for the change in fluorescence of prf-labeled tRNAs versus time are also in agreement with the experimental data of Pan et al. [16].

First, we study the temporal evolution of fMetPhe-puromycin formation. The results for the probability of posttranslocation state, $P_3(t)$, which characterizes the fraction of fMetPhe-puromycin formation, versus time at different EF-G-GTP concentrations are shown in

Fig. 3A. It is noted that the curve of $P_3(t)$ versus time at any [EF-G] can be approximately fit to a single exponential: $y = y_0 + Ae^{-kt}$, which is in agreement with the experimental data of Pan et al. [16]. Moreover, it is interesting to see that the curve of $P_3(t)$ versus time has a brief initial lag phase followed by a phase of exponential increase (see Fig. S2 in Supplementary material), which is consistent with the experimental data (Fig. 4C in Savelsbergh et al. [13]).

Then, we study the temporal evolution of fluorescence of prf-labeled tRNAs, which is calculated by Eq. (21). As discussed in the above section, to be consistent with the experimental data [16], it is required that $B_2/B_1 < 1.23$ for PRE complex 16/17A ($B_3/B_1 = 1.09$) at saturating EF-G.GTP. In Fig. S3 (see Supplementary material), we show *CF* versus time at [EF-G] = 5 μM, which is nearly saturated, for different values of $B_2/B_1 < 1.23$. It is noted that although the curve of *CF* versus time for any value of B_2/B_1 has the two-exponential form, it can be approximately fit to a single exponential: $y = y_0 + Ae^{-kt}$, and the rate k decreases with the decrease of B_2/B_1. When $B_2/B_1 = 1.05$, the rate $k = 7\ s^{-1}$, which is close to the experimental data of Pan et al. [16]. Thus, we infer that for PRE complex 16/17A, B_2/B_1 should be about 1.05, implying that the fluorescence intensity at the intermediate hybrid state (~1.05) is in between that of the non-rotated pretranslocation state (~1) and that of the posttranslocation state (~1.09). With $B_2/B_1 = 1.05$ and $B_3/B_1 = 1.09$, the calculated results of fluorescence intensity versus time at different EF-G.GTP concentrations are shown in Fig. 3B. It is interesting to see that the calculated results (Fig. 3B) are in good agreement with the experimental data (Fig. 1B in Pan et al. [16]).

For PRE complex 16/20A ($B_3/B_1 = 1.13$), at saturating EF-G.GTP it is required that $B_2/B_1 \geq 1.33$ for the maximum fluorescence intensity to exist that is larger than B_3 at $t = \infty$, as discussed in the above section. From the experimental data (see Fig. 1C in Pan et al. [16]), it is noted that the maximum fluorescence intensity is about 1.16 at [EF-G] = 5 μM, which is nearly saturated. On the other hand, from our theoretical data (Fig. 2B), it is seen that at saturating EF-G.GTP, $CF_{max} = 1.16$ occurs at about $B_2/B_1 = 1.55$. Thus, we infer that $B_2/B_1 = 1.55$ for PRE complex 16/20A in Pan et al. [16]. With $B_2/B_1 = 1.55$ and $B_3/B_1 = 1.13$, the calculated results of fluorescence intensity versus time at different EF-G.GTP concentrations are shown in Fig. 3C. It is seen that the curves in Fig. 3C resemble much the experimental data (Fig. 1C in Pan et al. [16]).

For PRE complex 20P ($B_3/B_1 = 0.9$), at saturating EF-G.GTP it is required that $B_2/B_1 > 1$ for the maximum fluorescence intensity to exist that is larger than B_1 at $t = 0$, as discussed in the above section. From the experimental data (see Fig. 1D in Pan et al. [16]), it is noted that the maximum fluorescence intensity is about 1.023 at [EF-G] = 5 μM, which is nearly saturated. From our theoretical data (Fig. 2B), it is seen that at saturating [EF-G], $CF_{max} = 1.023$ occurs at about $B_2/B_1 = 1.2$. Thus, with $B_2/B_1 = 1.2$ and $B_3/B_1 = 0.9$, the calculated results of fluorescence intensity versus time at different EF-G.GTP concentrations are shown in Fig. 3D. It is seen that curves in Fig. 3D resemble much the experimental data (Fig. 1D in Pan et al. [16]).

3.3. In the presence of EF-G.GDPNP

In our model, the difference between the effect of GDPNP and that of GTP on ribosomal translocation is that GTP hydrolysis facilitates the hybrid-to-posttranslocation transition. In other words, the ribosomal complex with the binding of EF-G.GDPNP has a smaller transition rate

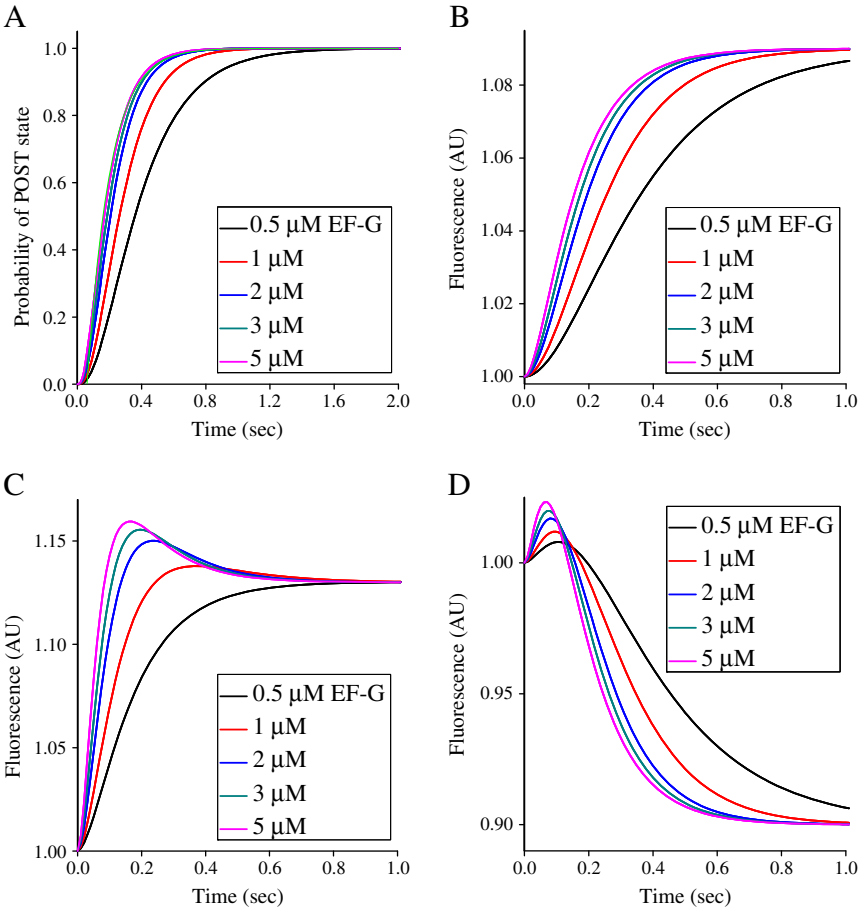

Fig. 3. EF-G.GTP-catalyzed tRNA–mRNA translocation. (A) Probability of posttranslocation state, $P_3(t)$, which characterizes the fraction of fMetPhe-puromycin formation, versus time at different EF-G-GTP concentrations, where green line is the fit curve to data at 5 μM EF-G.GTP with the single exponential: $y = y_0 + Ae^{-kt}$, where $k = 7\ s^{-1}$. (B)–(D) Fluorescence intensity versus time at different EF-G.GTP concentrations for three labeled PRE complexes 16/17A (B), 16/20A (C) and 20P (D).

k_2 than with the binding of EF-G.GTP, while the transition rates k_1, k_{-1} k_{10} and k_{-10} have nearly the same values for the two cases.

First, we study the temporal evolution of fluorescence of prf-labeled tRNAs at saturating EF-G.GDPNP and compare with that at saturating EF-G.GTP. For both GTP and GDPNP we take $k_1 = 8\ s^{-1}$ and $k_{-1} = 0.1\ s^{-1}$, while for GTP we take $k_2 = 20\ s^{-1}$ and for GDPNP we take $k_2 = 2\ s^{-1}$ (Table 1). The results of fluorescence intensity versus time are shown in Fig. 4A, where $B_2/B_1 = 1.1$ and $B_3/B_1 = 0.9$ for GTP and $B_2/B_1 = 1.01$ and $B_3/B_1 = 0.9$ for GDPNP. It is seen that the calculated results (Fig. 4A) resemble much the experimental data (inset of Fig. 3A in Pan et al. [16]). The slight difference in the value of B_2/B_1 with the binding of EF-G.GDPNP from that with the binding of EF-G.GTP could result from the slight difference between the conformation of the hybrid-state ribosomal complex when it is bound by EF-G.GDPNP and that when it is bound by EF-G.GTP or EF-G.GDP.Pi.

Then, we study the temporal evolution of fluorescence of prf-labeled tRNAs at non-saturating EF-G.GDPNP concentration. With $k_{10} = k_{-10} = 0.1\ s^{-1}$ and $k_b = 1\ \mu M^{-1}\ s^{-1}$, the calculated results of fluorescence intensity versus time at different EF-G.GDPNP concentrations are shown in Fig. 4B, where $B_2/B_1 = 1.05$ and $B_3/B_1 = 0.9$. It is seen that the curves in Fig. 4B resemble the experimental data (Fig. 3B in Pan et al. [16]).

4. Discussion

In this work, we proposed a simple model for the tRNA–mRNA translocation in the ribosome. The model was then formulated as a set of coupled linear differential equations, in order to provide quantitative explanations of the available experimental data which have not been quantitatively explained up to now. We showed that only this liner character of the model equations is sufficient to give a good quantitative explanation of the experimental data, without needing to resort to the non-linear character.

As mentioned in Introduction, a controversial issue concerning the mechanism of EF-G.GTP-catalyzed translocation is whether EF-G.GTP can bind to the non-rotated pretranslocation state. For example, Fei et al. [8] proposed that EF-G.GTP selectively binds to the hybrid state and does not bind to the non-rotated pretranslocation state, thus imparting directionality to the translocation reaction; while experimental data of Chen et al. [11] can be well explained by arguing that EF-G.GTP can bind to both the non-rotated pretranslocation and hybrid states. In the present work, using the model for tRNA–mRNA translocation through the ribosome, where EF-G.GTP can bind to both the non-rotated pretranslocation and the hybrid state, we showed that the theoretical results of fluorescence intensity versus time at different EF-G.GTP concentrations are in good agreement with the experimental data of Pan et al., [16]. Note that if EF-G.GTP can only bind to State C0, the calculated results are much similar to those (Fig. 3) for the case that EF-G.GTP can bind to both State C0 and State H0 (see Supplementary material). As the available experimental data showed, before the binding of EF-G the ribosomal complex can transit between the classical non-rotated pretranslocation and hybrid states [3–12]. Thus, the transitions between State C0 and State H0 are present in our model (Fig. 1). Moreover, the formation of the hybrid state is critical for the translocation to take place [4,28] and the EF-G-catalyzed translocation requires EF-G bound to the ribosomal pretranslocation complex, implying that EF-G is allowed to bind to the hybrid pretranslocation state. Thus, we argue that EF-G can bind to both State C0 and State H0. However, if we consider that EF-G.GTP can only bind to the hybrid state, our calculations show that the theoretical results are very different from the experimental data (see Supplementary material). Thus, our studies give a strong support to the argument that EF-G.GTP can also bind to the non-rotated pretranslocation besides the hybrid state, which is in agreement with the experimental data of Chen et al. [11].

It has been well determined that both the binding of EF-G.GTP and the binding of EF-G.GDPNP can activate the translocation of tRNA–mRNA and the translocation rate induced by the binding of EF-G.GTP is larger or much larger than by the binding of EF-G.GDPNP [12,14–18]. To explain their experimental data, Pan et al. [16] proposed that the faster rate induced by EF-G.GTP (i.e., GTP hydrolysis) than by EF-G.GDPNP results from the effects on the hybrid-state formation – the first step of tRNA–mRNA translocation process – rather than on the transition from the hybrid to posttranslocation state – the second step. However, recent experimental data by Ermolenko and Noller [18] evidently showed that the faster rate induced by EF-G.GTP than by EF-G.GDPNP results from the effects on the second step. This is consistent with the biochemical data showing that GTP hydrolysis accelerates the second step by promoting the ribosomal unlocking [13], which is supported by structural data [22,23]. However, no structural evidence is available to support the argument that GTP hydrolysis facilitates the first step. In the present work, in contrast to the explanation by Pan et al. [16], we explained that the greater potency of GTP hydrolysis in facilitating translocation of tRNA–mRNA complex derives from its effects on the second step rather than on the first step, thus giving a consistent explanation of both the experimental data of Pan et al. [16] and those of Ermolenko and Noller [18].

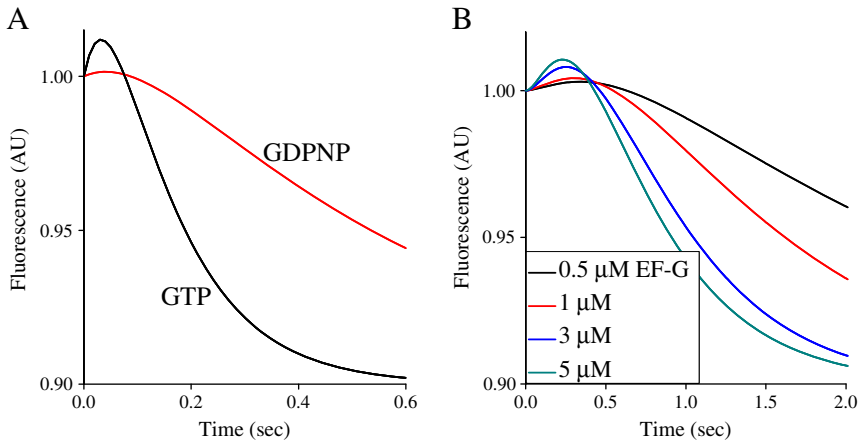

Fig. 4. EF-G.GDPNP-catalyzed tRNA–mRNA translocation. (A) Fluorescence intensity versus time at saturating EF-G.GDPNP for labeled PRE complex 20P, where, for comparison, the fluorescence intensity versus time at saturating EF-G.GTP for labeled PRE complex 20P is also shown. (B) Fluorescence intensity versus time at different EF-G.GDPNP concentrations for labeled PRE complex 20P.

Appendix A. Supplementary data

Supplementary data to this article can be found online at http://dx.doi.org/10.1016/j.bpc.2013.06.001.

References

[1] H.F. Noller, M.M. Yusupov, G.Z. Yusupova, A. Baucom, J.H.D. Cate, Translocation of tRNA during protein synthesis, FEBS Letters 514 (2002) 11–16.
[2] J. Frank, H. Gao, J. Sengupta, N. Gao, D.J. Taylor, The process of mRNA–tRNA translocation, Proceedings of the National Academy of Sciences of the United States of America 104 (2007) 19671–19678.
[3] D. Moazed, H.F. Noller, Intermediate states in the movement of transfer RNA in the ribosome, Nature 342 (1989) 142–148.
[4] R. Lill, J.M. Robertson, W. Wintermeyer, Binding of the 30-terminus of tRNA to 23S rRNA in the ribosomal exit site actively promotes translocation, EMBO Journal 8 (1989) 3933–3938.
[5] S.C. Blanchard, H.D. Kim, R.L. Gonzalez Jr., J.D. Puglisi, S. Chu, tRNA dynamics on the ribosome during translation, Proceedings of the National Academy of Sciences of the United States of America 101 (2004) 12893–12898.
[6] D.N. Ermolenko, Z.K. Majumdar, R.P. Hickerson, P.C. Spiegel, R.M. Clegg, F. Harry, H.F. Noller, Observation of intersubunit movement of the ribosome in solution using FRET, Journal of Molecular Biology 370 (2007) 530–540.
[7] J.B. Munro, R.B. Altman, N. O'Connor, BlanchardS.C. , Identification of two distinct hybrid state intermediates on the ribosome, Molecular Cell 25 (2007) 505–517.
[8] J. Fei, P. Kosuri, D.D. MacDougall, R.L. Gonzalez Jr., Coupling of ribosomal L1 stalk and tRNA dynamics during translation elongation, Molecular Cell 30 (2008) 348–359.
[9] P.V. Cornish, D.N. Ermolenko, H.F. Noller, T. Ha, Spontaneous intersubunit rotation in single ribosomes, Molecular Cell 30 (2008) 578–588.
[10] M. Valle, A. Zavialov, J. Sengupta, U. Rawat, M. Ehrenberg, J. Frank, Locking and unlocking of ribosomal motions, Cell 114 (2003) 123–134.
[11] C. Chen, B. Stevens, J. Kaur, D. Cabral, H. Liu, Y. Wang, H. Zhang, G. Rosenblum, Z. Smilansky, Y.E. Goldman, B. Cooperman, Single-molecule fluorescence measurements of ribosomal translocation dynamics, Molecular Cell 42 (2011) 367–377.
[12] A.V. Zavialov, M. Ehrenberg, Peptidyl-tRNA regulates the GTPase activity of translation factors, Cell 114 (2003) 113–122.
[13] A. Savelsbergh, V.I. Katunin, D. Mohr, F. Peske, M.V. Rodnina, W. Wintermeyer, An elongation factor G-induced ribosome rearrangement precedes tRNA–mRNA translocation, Molecular Cell 11 (2003) 1517–1523.
[14] M.V. Rodnina, A. Savelsbergh, V.I. Katunin, W. Wintermeyer, Hydrolysis of GTP by elongation factor G drives tRNA movement on the ribosome, Nature 385 (1997) 37–41.
[15] V.I. Katunin, A. Savelsbergh, M.V. Rodnina, W. Wintermeyer, Coupling of GTP hydrolysis by elongation factor G to translocation and factor recycling on the ribosome, Biochemistry 41 (2002) 12806–12812.
[16] D. Pan, S.V. Kirillov, B.S. Cooperman, Kinetically competent intermediates in the translocation step of protein synthesis, Molecular Cell 25 (2007) 519–529.
[17] C. Ticu, R. Nechifor, B. Nguyen, M. Desrosiers, K.S. Wilson, Conformational changes in switch I of EF-G drive its directional cycling on and off the ribosome, EMBO Journal 28 (2009) 2053–2065.
[18] D.N. Ermolenko, H.F. Noller, mRNA translocation occurs during the second step of ribosomal intersubunit rotation, Nature Structural & Molecular Biology 18 (2011) 457–463.
[19] P.C. Spiegel, D.N. Ermolenko, H.F. Noller, Elongation factor G stabilizes the hybrid-state conformation of the 70S ribosome, RNA 13 (2007) 1473–1482.
[20] J.S. Feinberg, S. Joseph, Identification of molecular interactions between P-site tRNA and the ribosome essential for translocation, Proceedings of the National Academy of Sciences of the United States of America 98 (2001) 11120–11125.
[21] P. Xie, Model of ribosome translation and mRNA unwinding, European Biophysics Journal 42 (2013) 347–354.
[22] B.S. Schuwirth, M.A. Borovinskaya, C.W. Hau, W. Zhang, A. Vila-Sanjurjo, J.M. Holton, J.H.D. Cate, Structures of the bacterial ribosome at 3.5 Å resolution, Science 310 (2005) 827–834.
[23] D.J. Taylor, J. Nilsson, A.R. Merrill, G.M. Andersen, P. Nissen, J. Frank, Structures of modified eEF2.80S ribosome complexes reveal the role of GTP hydrolysis in translocation, EMBO Journal 26 (2007) 2421–2431.
[24] W. Wintermeyer, F. Peske, M. Beringer, K.B. Gromadski, A. Savelsbergh, M.V. Rodnina, Mechanisms of elongation on the ribosome: dynamics of a macromolecular machine, Biochemical Society Transactions 32 (2004) 733–737.
[25] H.D. Kim, J. Puglisi, S. Chu, Fluctuations of tRNAs between classical and hybrid states, Biophysical Journal 104 (2007) 13661–13665.
[26] S. Uemura, C.E. Aitken, J. Korlach, B.A. Flusberg, S.W. Turner, J.D. Puglisi, Real-time tRNA transit on single translating ribosomes at codon resolution, Nature 464 (2010) 1012–1017.
[27] P. Xie, Dynamics of tRNA occupancy and dissociation during translation by the ribosome, Journal of Theoretical Biology 316 (2013) 49–60.
[28] L.H. Horan, H.F. Noller, Intersubunit movement is required for ribosomal translocation, Proceedings of the National Academy of Sciences of the United States of America 104 (2007) 4881–4885.